ATMOSPHERIC AND OCEANIC SCIENCE LETTERS, 2010, VOL. 3, NO. 1, 7–13

Modeling Gross Primary Production by Integrating Satellite Data and Coordinated Flux Measurements in Arid and Semi-Arid China

WANG He-Song[1,2], JIA Gen-Suo[1], FENG Jin-Ming[1], ZHAO Tian-Bao[1], and MA Zhu-Guo[1]

[1] *Key Laboratory of Regional Climate-Environment Research for Temperate East Asia, Institute of Atmospheric Physics, Chinese Academy of Sciences, Beijing 100029, China*
[2] *Graduate University of Chinese Academy of Sciences, Beijing 100049, China*

Received 30 October 2009; revised 12 December 2009; accepted 18 December 2009; published 16 January 2010

Abstract Assessing large-scale patterns of gross primary production (GPP) in arid and semi-arid (ASA) areas is important for both scientific and practical purposes. Remote sensing-based models, which integrate satellite data with input from ground-based meteorological measurements and vegetation characteristics, improve spatially extended estimates of vegetation productivity with high accuracy. In this study, the authors simulated GPP in ASA areas by integrating moderate resolution imaging spectral radiometer (MODIS) data with eddy covariance and meteorological measurements at the flux tower sites using the Vegetation Photosynthesis Model (VPM), which is a remote sensing-based model for analyzing the spatial pattern of GPP in different land cover types. The field data were collected by coordinating observations at nine stations in 2008. The results indicate that in the region during the growing season GPP was highest in cropland sites, second highest in woodland sites, and lowest in grassland sites. VPM captured the temporal and spatial characteristics of GPP for different land covers in ASA areas. Further, Enhanced Vegetation Index (EVI) had a strong liner relationship with GPP in densely vegetated areas, while the Normalized Difference Vegetation Index (NDVI) had a strong liner relationship with GPP over less dense vegetation. This study demonstrates the potential of satellite-driven models for scaling-up GPP, which is a key component for studying the carbon cycle at regional and global scales.

Keywords: gross primary production, vegetation photosynthesis model, eddy covariance, remote sensing, coordinated observation, arid and semi-arid areas

Citation: Wang, H.-S., G.-S. Jia, J.-M. Feng, et al., 2010: Modeling gross primary production by integrating satellite data and coordinated flux measurements in arid and semi-arid China, *Atmos. Oceanic Sci. Lett.*, **3**, 7−13.

1 Introduction

Arid and semi-arid (ASA) areas comprise about 30%–45% of the earth's surface and cover more than one-third of China's mainland (Liu et al., 2008). The interaction processes between land and atmosphere in ASA areas are important because of the high sensible heat flux and the increasing aridification and desertification over the past decades (Fu and An, 2002; Huenneke et al., 2002). Meanwhile, semi-arid areas are more sensitive to climate change and human disturbances (Fu and Wen, 2002). The gross primary production (GPP) of vegetation is a key component of land-atmosphere interaction, determines the strength of the carbon sink of terrestrial ecosystems. Assessing large-scale patterns of GPP in ASA areas is important for both scientific and practical purposes.

Field-based continuous measurements from fixed platforms, such as eddy covariance (EC) flux towers, is one of the most useful micrometeorological methods for estimating the carbon exchange between terrestrial ecosystems and the atmosphere (Li et al., 2007). However, EC measurements only represent the fluxes within its own footprint, which can be up to several square kilometers over a heterogeneous land surface (Xiao et al., 2008). It remains a challenging task to extrapolate EC measurements from sparsely distributed flux towers to meaningful vegetation parameters at the regional scale.

Satellite remote sensing has greatly enhanced the global and regional scale observations of vegetation dynamics, and has played an increasing role in scaling EC measurements to large areas (Running et al., 2004; Turner et al., 2005; Garbulsky et al., 2008). Remote sensing based models employ inputs from ground based meteorological measurements (including air temperature, vapor-pressured deficit (VPD), and photosynthetic active radiation (PAR)) and vegetation characteristics (including vegetation type, vegetation fraction, and light use efficiency (LUE)) to improve the accuracy of GPP or Net Primary Productivity (NPP) estimation. An integrated method of remote sensing and flux measurements would be extremely helpful for improving spatially extended estimates of vegetation productivity with high accuracy.

The Vegetation Photosynthesis Model (VPM), a remote sensing-based model, has been recently developed by Xiao et al. (2004a, b). VPM has successfully demonstrated its potential for scaling-up GPP from flux tower sites to the regional scale by integrating remote sensing and flux measurements. The VPM model has been rigorously evaluated with data from a single flux tower that made measurements in temperate deciduous, broadleaf forest, evergreen coniferous forest, seasonally moist tropical forest, alpine meadow, managed croplands and old-growth temperate mixed forest sites (Xiao et al., 2004a, b, 2005a, b; Li et al., 2007; Yan et al., 2009; Wu et al., 2009). However, the application of VPM to ASA areas

Corresponding author: JIA Gen-Suo, jiong@tea.ac.cn

over complicated land surfaces and its validation with coordinated multi-site flux observations in different land cover types are still lacking. The goal of this study was to determine whether VPM has the ability to describe the characteristics of GPP in different land cover types in ASA areas of China. Specifically, the objectives of this study were the following: (1) to study the characteristics of GPP in different land cover types in ASA areas of China; (2) to evaluate the VPM modeled GPP by comparison with the EC measured GPP in different land cover types of China's ASA areas; and (3) to compare the relationship between the vegetation indices (Enhanced Vegetation Index (EVI) and the Normalized Difference Vegetation Index (NDVI)) and GPP. Finally, the potential of satellite remote sensing for studying and monitoring vegetation and carbon fluxes in ASA areas of China will be explored.

2 Data and methods

2.1 Description of study sites

We chose nine sites from the coordinated enhanced observation project in ASA areas of China (Table 1). These nine flux sites are representative of the following dominant land cover types found in ASA areas of northern China: temperate grassland, cropland, deciduous broadleaf forests, and evergreen needleleaf forests. Jinzhou (JZ), Linze (LZ), and Yingke (YK) are all irrigated cropland sites of maize with intensive management. Dayekou (DYK) is a sub-alpine evergreen needleleaf forest site, while Changwu (CW) and Miyun (MY) are deciduous broadleaf forest sites. Arou (AR) is a sub-alpine meadow site, and Dongsu (DS) represents desert steppe, while Tongyu (TY) represents degraded meadow site.

2.2 Coordinated measurements and data corrections

Carbon flux and meteorological data sets were collected from the nine sites described above. The EC systems were mounted above the canopy from 1 m to 25 m (Table 1) and consisted of a three-dimensional sonic anemometer and an open-path fast response infrared gas analyzer. Intensive calibration was performed in June 2008, directly before the coordinated observation period (July to September, 2008) to ensure optimal performance of the instruments and that measurements at all participant sites were comparable. The Webb-Pearman-Leuning (WPL) correction, which compensates for the fluctuations of temperature and water vapor that affect the measured fluctuations of CO_2 and H_2O, was applied to the net ecosystem exchange (NEE) measurements (Webb et al., 1980). Data points that were compromised by moisture condensation and rain droplets on the windows of the infrared gas analyzer were removed. A linear interpolation method was applied to fill small blocks (less than two hours) of missing or bad data. Larger gaps were filled with values derived from mean diurnal ensemble values (Fagle et al., 2001). More details on data treatments have been described by Liu et al. (2008).

During nighttime, NEE was treated as ecosystem respiration because photosynthesis equals zero. Daytime ecosystem respiration was estimated based on the relationship between nighttime respiration and soil temperature to daytime (Hu et al., 2008). Finally, GPP was estimated as NEE minus the estimated daytime ecosystem respiration ($R_{\text{Day-eco}}$):

$$\text{GPP} = \text{NEE} - R_{\text{Day-eco}} . \quad (1)$$

Then, daily GPP values calculated above were averaged to eight-day intervals to be consistent with the Moderate Resolution Imaging Spectroradiometer (MODIS) eight-day composites.

2.3 Description of VPM

The VPM algorithm was described in detail by Xiao et al. (2004a, b). The algorithm is based on LUE, PAR, and the fraction of PAR absorbed by photosynthetic active vegetation (PAV, chloroplasts):

$$\varepsilon_g = \varepsilon_0 \times T_{\text{scalar}} \times W_{\text{scalar}} \times P_{\text{scalar}} , \quad (2)$$

$$\text{GPP} = \varepsilon_g \times \text{FAPAR}_{\text{PAV}} \times \text{PAR} , \quad (3)$$

where ε_0 is maximal light use efficiency. T_{scalar}, W_{scalar}, and P_{scalar} are the limiting scalars for the effects of temperature, water, and leaf phenology on LUE, respectively. $\text{FAPAR}_{\text{PAV}}$ is the fraction of PAR absorbed by PAV (chloroplasts), and ε_g is actual light use efficiency.

2.4 Estimation of VPM model parameters

In this study, ε_0 of the nine flux sites were calculated using the Michaelis-Menten light response function:

Table 1 Location and characteristics of the nine flux sites in ASA region of northern China.

Site	Land cover	Location	EC above canopy (m)	Annual precipitation (mm)	Elevation(m)
JZ	Cropland	41°08.9′N, 121°12.1′E	1	463	17
YK	Cropland	38°51.4′N, 100°15.0′E	1	382	2859
LZ	Cropland	39°19.7′N, 100°24.6′E	1	376	1382
DYK	Woodland	38°32.0′N, 100°15.0′E	2	360	2823
CW	Woodland	35°14.5′N, 107°40.9′E	20	540	1220
MY	Woodland	40°37.9′N, 117°19.4′E	25	584	350
DS	Grassland	44°05.3′N, 113°34.5′E	2	287	990
TY	Grassland	44°34.0′N, 122°55.2′E	2	404	151
AR	Grassland	38°02.7′N, 100°27.9′E	2	396	3033

$$\mathrm{GPP} = \frac{\varepsilon_0 \times \mathrm{PAR} \times \mathrm{GPP}_{\max}}{\varepsilon_0 \times \mathrm{PAR} + \mathrm{GPP}_{\max}}, \quad (4)$$

where $\mathrm{GPP}_{\max}$ is the maximal GPP.

T_{scalar} is estimated from the equation of the minimal, maximal, and optimal temperature for photosynthesis. Information about the retrieved ε_0 and the temperature sets for the calculation of T_{scalar} are listed in Table 2. In this study, P_{scalar} is set to 1 because all vegetation types had new leaves emerging throughout the growing season.

W_{scalar} and $\mathrm{FAPAR}_{\mathrm{PAV}}$ were calculated from Land Surface Water Index (LSWI) and EVI, respectively. LSWI and EVI were generated from MOD09A1 provided by the MODIS Land Science Team with eight-day intervals (http://modis-land.gsfc.nasa.gov/). We selected 3×3 subsets (approximately 1.5×1.5 km^2) of MOD09A1 corresponding to the period of the coordinated flux measurements that were centered on the eddy flux tower sites of this study from the Oak Ridge National Laboratory (ORNL, http://www.modis.ornl.gov/modis/index.cfm).

LSWI is sensitive to changes in leaf water content over time (Maki et al., 2004):

$$\mathrm{LSWI} = \frac{\rho_{\mathrm{nir}} - \rho_{\mathrm{swir}}}{\rho_{\mathrm{nir}} + \rho_{\mathrm{swir}}}, \quad (5)$$

where ρ_{swir} is the reflectance in the short infrared band (1628–1652 nm), and ρ_{nir} is the reflectance in near infrared band (841–876 nm).

EVI includes the blue band for atmospheric, soil, and canopy background signal correction and has recently been used for the study of vegetation greenness (Zhang et al., 2003; Boles et al., 2004):

$$\mathrm{EVI} = \frac{G \times (\rho_{\mathrm{nir}} - \rho_{\mathrm{red}})}{(\rho_{\mathrm{nir}} + (C_1 \times \rho_{\mathrm{red}} - C_2 \times \rho_{\mathrm{blue}}) + L)}, \quad (6)$$

where ρ_{red} is the reflectance in the red band (620–670 nm), ρ_{nir} is the reflectance in the near infrared band (841–876 nm), and ρ_{blue} is the reflectance in the blue band (459–479 nm). The coefficients adopted in the EVI algorithm are the following: L=1, C_1=6, C_2=7.5, and G (gain factor) =2.5 (Huete et al., 2002).

3 Results and discussion

3.1 Spatial patterns of EC measured GPP

The EC measured GPP ($\mathrm{GPP}_{\mathrm{pred}}$) varies among different land cover types as shown by the following coordinated field observations from July to September (Table 3): the GPP of cropland sites had the highest values, ranging from 715.22 gC m^{-2} to 866.48 gC m^{-2}; Woodland sites took the second place, ranging from 353.1 gC m^{-2} to 596.9 gC m^{-2}; and Grassland sites had the lowest GPP value, ranging from 79.44 gC m^{-2} to 347.59 gC m^{-2}.

Table 2 Parameters from the nine flux sites in ASA areas of northern China for VPM modeling.

Site	Type	$T_{\min}$ (°C)	T_{opt} (°C)	$T_{\max}$ (°C)	ε_0 (gC mol PAR^{-1})
JZ	Cropland	8	30	42	0.78
YK	Cropland	8	30	42	0.53
LZ	Cropland	8	30	42	0.51
DYK	Woodland	0	24	38	0.57
CW	Woodland	0	24	38	0.39
MY	Woodland	0	24	38	0.65
DS	Grassland	2	25	35	0.17
TY	Grassland	2	25	35	0.39
AR	Grassland	2	25	35	0.47

Table 3 Comparison of sums (from July to September), relative errors, correlations, and significances of $\mathrm{GPP}_{\mathrm{obs}}$ and $\mathrm{GPP}_{\mathrm{pred}}$ at the nine flux sites in ASA areas of northern China.

Site	Type	Sum of $\mathrm{GPP}_{\mathrm{obs}}$	Sum of $\mathrm{GPP}_{\mathrm{pred}}$	Relative errors (RE, %)*	Correlations (R^2)	Significance (p)
JZ	Cropland	866.48	922.53	6.47	0.64	<0.01
YK	Cropland	715.22	707.70	–1.05	0.92	<0.01
LZ	Cropland	785.55	795.20	1.23	0.90	<0.01
DYK	Woodland	353.10	299.28	–15.24	0.67	<0.01
CW	Woodland	362.93	381.49	5.11	0.86	<0.01
MY	Woodland	596.90	730.62	22.40	0.74	<0.01
DS	Grassland	79.44	77.50	–2.45	0.33	<0.05
TY	Grassland	313.01	367.62	17.00	0.67	<0.01
AR	Grassland	347.59	308.37	–11.28	0.92	<0.01

*RE= $[(\mathrm{GPP}_{\mathrm{obs}} - \mathrm{GPP}_{\mathrm{pred}}) / \mathrm{GPP}_{\mathrm{obs}}] \times 100\%$.

These distinct patterns in GPP variation among different land cover types can be explained, in part, by factors discussed forthwith. The cropland sites were all cultivated with maize, a C4 plant that has a greater LUE than the C3 plants that dominate other land cover types in ASA areas (Lobell et al., 2002). Meanwhile, cropland irrigation greatly reduced the water deficit that often limits the productivity of natural vegetation in ASA areas. Croplands had the highest GPP in summer, however, their short turnover period undermined their function as a carbon sink. At the woodland sites, MY had the highest GPP, perhaps because it had higher rainfall than the other woodland sites. CW had similar water and temperature conditions to MY, however, its low fraction of woodland likely caused its GPP to be lower than MY. DYK was highly limited by both temperature and water supply likely because of its high elevation and low rainfall. There were great differences in GPP among the grassland sites. The desert steppe site, DS, had the lowest GPP largely because of its large water supply limitation, whereas the GPP of the typical steppe site, TY, was higher, but was still water limited. The alpine meadow site, AR, had the highest GPP among the grassland sites, largely because its moisture condition was more optimal in the high elevation area.

3.2 Evaluation of VPM modeled GPP

The VPM model was run using the vegetation indices, site-specific air temperature, and PAR data over each flux site. We compared the dynamics of VPM simulated GPP (GPP_{pred}) with EC measured GPP (GPP_{obs}) over the coordinated enhanced observation period for each site (Fig. 1). Generally, GPP_{pred} and GPP_{obs} had similar trends during the growing season and were highly correlated at all flux sites, except DS (Table 3), which was heavily limited by water supply and had the lowest GPP value among all sites. This indicates that VPM might have lower sensitivity to areas with extremely low vegetation productivity.

The liner regression model also showed reasonable agreement among different land cover types (Fig. 2). For data from all land cover types, the correlation was in good agreement and was highly significant (R^2=0.90, p<0.01). For comparisons of data within a single land cover type, these sites also had highly significant correlations (R^2=0.85, 0.85, and 0.81 for grassland, woodland, and cropland, respectively).

In general, the relative errors of all sites were within the range of ±20%, except for MY (Table 3). MY is a woodland site in a hilly region and its GPP_{pred} was 22.4% higher than GPP_{obs}. The large footprint of this site, because of its high EC platform, included areas of bare soil or sparsely vegetated areas. The GPP_{obs} of this site was decreased by the surrounding low productivity vegetation. This caused an overestimation of GPP as modeled by VPM, which simulates GPP from the input of pixels with high vegetation dynamics around the flux towers. GPP_{obs} depends strongly on the footprint, which relies on weather conditions (Schmid, 2002) and the height of platform. Consequently, GPP_{obs} might be influenced by the heterogeneous land cover types surrounding the flux site. This indicates that the spatial mismatch of representative areas between flux measurements and remote sensing estima-

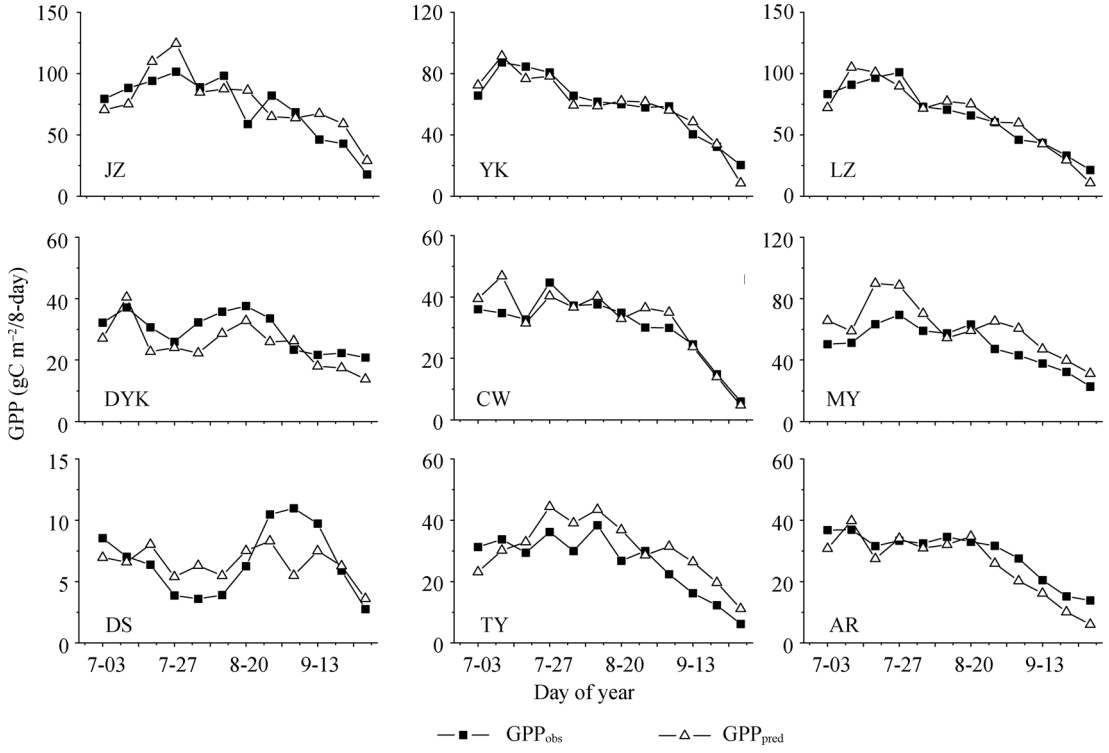

Figure 1 Dynamics of eddy covariance technique (EC) measured GPP (GPP_{obs}) and VPM predicted GPP (GPP_{pred}) from the nine sites in arid and semi-arid (ASA) areas of northern China in growing season (July to September, 2008).

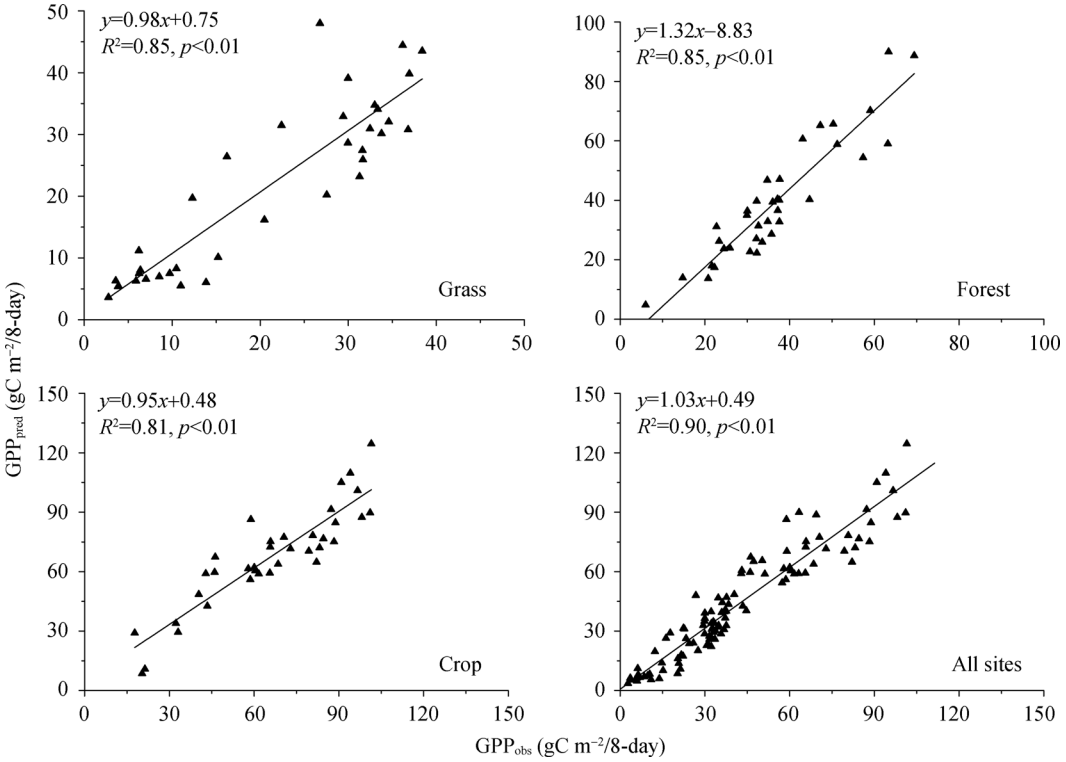

Figure 2 Comparison between GPP_{obs} and GPP_{pred} in different land cover types and for all sites combined in ASA areas of northern China during the growing season (July to September, 2008).

tions is a potential source of disagreement between GPP_{obs} and GPP_{pred} at any site.

3.3 Correlations between GPP and vegetation indices

The correlations between the vegetation indices (EVI, NDVI) and GPP_{obs} present different patterns in different land cover types (Fig. 3). Grassland and cropland sites exhibited higher correlations, likely because of their relatively homogeneous vegetation at pixel scale. The EC towers were all mounted above flat and open surfaces. However, woodland sites had lower correlations likely because of the complex terrain. Combining all the sites, the correlations were also low. This indicates that a simple liner regression between Vegetation Indice (VIs) and GPP is likely only suitable for certain or for similar vegetation type sites, but might not work well for sites with complicated vegetation types at the pixel scale.

When comparing EVI with NDVI, EVI had a stronger linear relationship with GPP than NDVI did for all sites combined. The same pattern was also found within woodland and grassland sites; however, in low production areas, such as grassland sites, NDVI had higher correlations with GPP than EVI. This is not consistent with previous studies, which reported that EVI had stronger liner relationship with GPP than NDVI. However, those studies were conducted mainly in high GPP areas such as forests and croplands (Xiao et al., 2004a, b; Li et al., 2007; Wu et al., 2009). In high GPP areas, EVI had a stronger liner relationship likely due to its greater sensitivity to high biomass regions. In low GPP areas, NDVI had a wider range than EVI; thus, NDVI was more sensitive to low biomass areas.

4 Conclusion

In situ measurements of land surface processes in ASA areas of northern China are becoming a new focus as increasing numbers of observational sites are established. It is critical, but challenging, to scale up those valuable measurements for a larger picture at the regional scale. In this study, we calibrated EC instruments, performed quality control methods to improve data quality, measured the carbon fluxes over the nine sites in summer of 2008 and attempted to simulate and analyze regional patterns of GPP using a remote sensing based vegetation model. The ability of VPM to estimate GPP in different land cover types of ASA areas in northern China was investigated. The spatial analysis of GPP_{obs} indicated that during the growing season GPP was highest in cropland sites, second highest in woodland sites, and lowest in grassland sites in the region. VPM was found to adequately characterize the spatial pattern of GPP for different land cover types in ASA areas. The relationship between vegetation indices (EVI and NDVI) and GPP were compared and it was determined that EVI had stronger liner relationship with GPP, mainly in high biomass regions, while NDVI had stronger liner relationship with GPP in low biomass regions. Our study demonstrated the potential of VPM for scaling flux measurements to the regional scale in ASA areas.

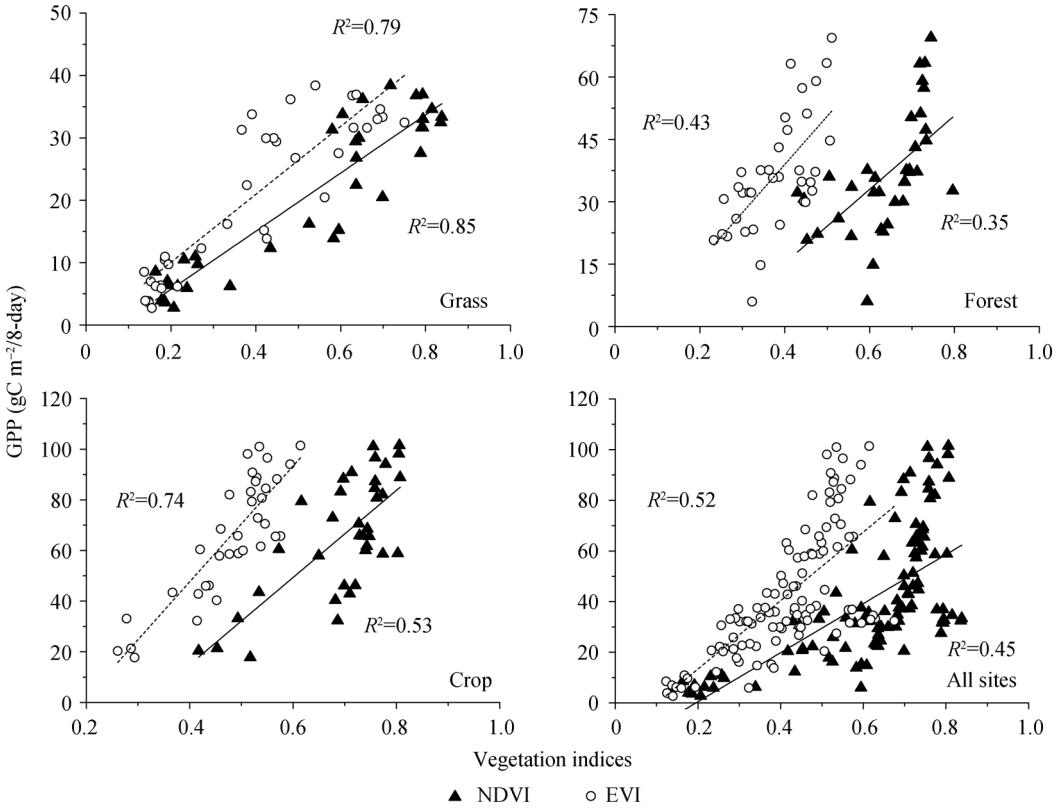

Figure 3 Simple linear regression analyses between EC measured GPP and vegetation indices (NDVI, EVI) for data in different land cover types and all sites combined. Dashed line is regression analysis between GPP and EVI (R^2=0.79, 0.43, 0.74, and 0.52 for grass sites, woodland sites, crop sites, and all sites combined, respectively), and solid line is regression analysis between GPP and NDVI (R^2=0.85, 0.35, 0.53, and 0.45 for grass sites, woodland sites, crop sites, and all sites combined, respectively).

Acknowledgements. This study was supported by the National Basic Research Program of China (Grant Nos. 2009CB723904 and 2006CB400500). We thank Professor FU Congbin for his valuable suggestions on this study and manuscript. The field measurements of GPP were provided by nine participant flux sites under the Enhanced Coordinated Observation in Arid and Semi-Arid China project.

References

Boles, S. H., X.-M. Xiao, J.-Y. Liu, et al., 2004: Land cover characterization of Temperate East Asia using multi-temporal VEGETATION sensor data, *Remote Sens. Environ.*, **90**, 477–489.

Fagle, E., D. Baldocchi, R. Olson, et al., 2001: Gap filling strategies for defensible annual sums of net ecosystem exchange, *Agric. Forest Meteor.*, **107**, 43–69.

Fu, C.-B., and Z.-S. An, 2002: Study of aridication in northern China—A global change issue forcing directly the demand of nation, *Earth Sci. Front.* (in Chinese), **9**, 271–275.

Fu, C.-B., and G. Wen, 2002: Several issues on aridication in the northern China, *Climatic Environ. Res.* (in Chinese), **7**, 22–29.

Garbulsky, M. F., J. Penuelas, D. Papale, et al., 2008: Remote estimation of carbon dioxide uptake by a Mediterranean forest, *Global Change Biol.*, **14**, 2860–2867.

Hu, Z., G. Yu, Y. Fu, et al., 2008: Effects of vegetation control on ecosystem water use efficiency within and among four grassland ecosystems in China, *Global Change Biol.*, **14**, 1609–1619.

Huenneke, L. F., J. P. Anderson, M. Remmenga, et al., 2002: Desertication alters patterns of aboveground net primary production in Chihuahuan ecosystems, *Global Change Biol.*, **8**, 247–264.

Huete, A., K. Didan, T. Miura, et al., 2002: Overview of the radiometric and biophysical performance of the MODIS vegetation indices, *Remote Sens. Environ.*, **83**, 195–213.

Li, Z.-Q., G.-R.Yu, X.-M. Xiao, et al., 2007: Modeling gross primary production of alpine ecosystems in the Tibetan Plateau using MODIS images and climate data, *Remote Sens. Environ.*, **107**, 510–519.

Liu, H.-Z., G. Tu, C.-B. Fu, et al., 2008: Three-year variations of water, energy and fluxes of cropland and degraded grassland surfaces in a semi-arid area of northeastern China, *Adv. Atmos. Sci.*, **25**(6), 1009–1020.

Lobell, D. B., J. A. Hicke, G. P. Asner, et al., 2002: Satellite estimates of productivity and light use efficiency in United States agriculture, 1982–98, *Global Change Biol.*, **8**, 722–735.

Maki, M., M. Ishiahra, and M. Tamura, 2004: Estimation of leaf water status to monitor the risk of forest fires by using remotely sensed data, *Remote Sens. Environ.*, **90**, 441–450.

Running, S. W., R. R. Nemani, F. A. Heinsch, et al., 2004: A continuous satellite-derived measure of global terrestrial primary production, *Bioscience*, **54**, 547–560.

Schmid, H. P., 2002: Footprint modeling for vegetation atmosphere exchange studies: A review and perspective, *Agric. Forest Meteor.*, **113**, 159–183.

Turner, D. P., W. D. Ritts, W. B. Cohen, et al., 2005: Site-level evaluation of satellite-based global terrestrial gross primary production and net primary production monitoring, *Global Change Biol.*, **11**, 666–684.

Webb, E. K., G. I. Pearman, and R. Leuning, 1980: Correction of flux measurements for density effects due to heat and water vapour transfer, *Quart. J. Roy. Meteor. Soc.*, **106**, 85–100.

Wu, J.-B., X.-M. Xiao, D.-X. Guan, et al., 2009: Estimation of the gross primary production of an old-growth temperate mixed forest using eddy covariance and remote sensing, *Int. J. Remote Sens.*, **30**, 463–479.

Xiao, J.-F., Q.-L. Zhuang, D. D. Baldocchi, et al., 2008: Estimation of net ecosystem carbon exchange for the conterminous United

States by combining MODIS and AmeriFlux data, *Agric. Forest Meteor.*, **148**, 1827–1847.

Xiao, X.-M., D. Hollinger, J. Aber, et al., 2004a: Satellite-based modeling of gross primary production in an evergreen needleleaf forest, *Remote Sens. Environ.*, **89**, 519–534.

Xiao, X.-M., Q.-Y. Zhang, B. Braswell, et al., 2004b: Modeling gross primary production of temperate deciduous broadleaf forest using satellite images and climate data, *Remote Sens. Environ.*, **91**, 256–270.

Xiao, X.-M., Q.-Y. Zhang, D. Hollinger, et al., 2005a: Modeling gross primary production of an evergreen needleleaf forest using MODIS and climate data, *Ecol. Appl.*, **15**, 954–969.

Xiao, X.-M., Q.-Y. Zhang, S. Saleska, et al., 2005b: Satellite-based modeling of gross primary production in a seasonally moist tropical evergreen forest, *Remote Sens. Environ.*, **94**, 105–122.

Yan, H.-M., Y.-L. Fu, X.-M. Xiao, et al., 2009: Modeling gross primary productivity for winter wheat-maize double cropping System using MODIS time series and CO2 eddy flux tower data, *Agric., Ecosyst. Environ.*, **129**, 391–400.

Zhang, X. Y., M. A. Friedl, C. B. Schaaf, et al., 2003: Monitoring vegetation phenology using MODIS, *Remote Sens. Environ.*, **84**, 471–475.